JOINT EUROPEAN TORUS

JET–P(85)07

P.H. Rebut, R.J. Bickerton
and B.E. Keen

The Joint European Torus (JET): Installation, First Results and Prospects

The Joint European Torus (JET): Installation, First Results and Prospects

P.H. Rebut, R.J. Bickerton
and B.E. Keen

JET-Joint Undertaking, Culham Science Centre, OX14 3DB, Abingdon, UK

Preprint of Paper to be submitted for publication in
Nuclear Fusion 25th Anniversary Issue (September 1985)

THE JOINT EUROPEAN TORUS: INSTALLATION, FIRST RESULTS AND PROSPECTS

P H Rebut, R J Bickerton and B E Keen

JET Joint Undertaking, Abingdon, Oxon, OX14 3EA. UK

I INTRODUCTION

The Joint European Torus (JET) is the largest single project of the nuclear fusion research programme of the European Atomic Energy Community (EURATOM). The project was designed with the essential objective of obtaining and studying plasma in conditions and with dimensions approaching those needed in a fusion reactor. The studies are aimed at:

a) investigating plasma processes and scaling laws as plasma dimensions and parameters approach those necessary for a fusion reactor;

b) examining and controlling plasma-wall interactions and impurity influxes in near-reactor conditions;

c) demonstrating effective heating techniques, capable of approaching reactor temperatures in JET, in the presence of the prevailing loss processes (particularly, R.F. and Neutral Beam Heating processes);

d) studying alpha-particle production, confinement and subsequent plasma interaction and heating produced as a result of fusion between deuterium and tritium.

II MACHINE DESIGN AND PARAMETERS

Following an initial design stage [1], a decision was taken in 1978 to build JET and that it should be located on the Culham Laboratory (U.K.) site. The machine (see Fig. 1) was ready for operation in June 1983. This large tokamak device has overall dimensions of about 15m diameter and 12m high; the other principal parameters are shown in Table I. The basic construction is intended to provide a varying D-shaped cross-section plasma of large volume (up to $190m^3$), with plasma currents up to 4.8MA contained within a toroidal magnetic field (up to 3.45T), into which further heating power (up to 15MW R.F. and 10MW neutral beam) can be added. If the heating results and containment properties are sufficiently good, deuterium and tritium should be added in the final stages of the programme to carry out experiments with significant α - particle heating.

III MACHINE OPERATION

The vacuum vessel is a double walled structure made up of eight octants joined by bellows, all made in Inconel [2]. With this wall material, electropolishing the inner surface, and baking the vessel, a high quality vacuum is obtained. The main wall conditioning technique is through glow discharge cleaning (GDC) at vessel temperatures up to 300°C. Typical cleaning after opening involves a water rinse of the walls, pumping down, baking to 300°C for 48 hours and GDC for 72 hours. During GDC, the impurity partial pressure increases by several orders of magnitude and the gas is progressively pumped away. For operation, UHV conditions are typically $\sim 10^{-7}$ mbar total hydrogen pressure, with $\simeq 10^{-9}$ mbar residual impurities, primarily CH_4, H_2O and CO at the operating wall temperature of ~270°C. Pulse discharge cleaning (~ 12,000 shots, 0.5s duration at I_p = 40kA) was tried but no major improvement in subsequent plasma performance was achieved. Gas is introduced into the

vessel for plasma production through three introduction modules, each permitting fast puffing for prefilling, and controlled addition of gas during the current pulse. The valves are fully metallic and bakeable to 300°C.

Four graphite limiters (0.4m wide and 0.8m high) fixed inside the vessel on the outboard side of the equatorial plane define the outer plasma boundary. These are curved in the toroidal direction to accommodate plasmas of different scrape-off layers (1-3cm thick). Two limiters are observed by infra-red cameras. Typically surface temperatures reach values up to 1500°C during operations. The transition from near-circular plasmas ($b/a < 1.2$) to elliptical ones with elongations up to 1.6 show an increased plasma length interacting with the limiters and the scrape-off layer slightly broadened. Due to limiter shape, heating was localised at two zones on either side of the vertical line of symmetry. The separation of the two regions indicated a scrape-off layer thickness of about 1.4cm during the flat top and about 3cm during the current rise and fall phases; plasma flows behind the limiters have been observed during disruptions. With elongated plasmas, the scrape-off layer thickness increased by $\sim$ 50% probably due to the increased connection length.

Three feedback control systems have been used for plasma current and radial position control and for the stabilisation of the vertical position. A fourth system has been prepared for the control of the elongation ratio (b/a) of the plasma cross section. During early operational periods, the plasma current was controlled by preprogramming the excitation voltage of the poloidal flywheel generator convertor using a simplified simulation model of JET. This operational mode was generally satisfactory. Subsequently, a current feedback system was successfully introduced. This provides a more convenient way of achieving constant current flat-top pulses. The control error is <5%, and it can be further reduced by auxiliary preprogramming.

The radial position control uses the measured poloidal flux difference between that at the limiter and at the desired inboard position of the limiter magnetic surface (i.e. plasma boundary) as a feedback control signal to the power source of the vertical field coil. The inboard position can be varied during the pulse by pre-programming, for example, to build up the plasma starting from a small initial radial diameter. This system has worked satisfactorily. However, its response has been extended by doubling the voltage range of the vertical field power source in order to cope more easily with large amplitude perturbations, such as disruptions.

The vertical plasma position is intrinsically unstable due to both the quadrupole poloidal field needed for elongating the plasma and the destabilizing forces of the iron circuit. The position is stabilized using a feedback amplifier connected to a radial field coil. The feedback stabilizing system of the vertical plasma position is similar to the radial position control but requires a much smaller current response. Since a fast response time of the amplifier output voltage to a vertical position change is essential, the feedback controller includes a derivative stage for the measured radial poloidal flux, equivalent to velocity feedback of the vertical position. In early experiments, the plasma became vertically unstable, despite the feedback system, as stabilization limits were exceeded. These limits depend crucially on the response time of the radial field amplifier and on the feedback loop gain. On a simplified model, the onset of instability was expected when the loop growth rate exceeded a certain value. Theoretically, the growth rate in the absence of feedback increases with the elongation ratio, b/a, the mean plasma/vessel distance and with the relative width of the current profile. Subsequent experiments confirmed these predictions.

In one case, at an elongation of 1.7, the plasma became vertically unstable at $I_p \sim 2.7$MA and moved downwards by 1m in 30ms without significant current change, followed by a radial inward movement of 0.8 m and a current quench lasting 25ms. Measurements indicated that the poloidal fields generated by eddy currents in the vessel and in the radial field coil were insufficient to maintain equilibrium. Additional poloidal currents across the plasma, returning through the vessel, were needed. The vacuum vessel experienced violent mechanical forces in excess of 200t, leading to transient displacements of several mm. Since these forces scale as I_p^2, loss of vertical stabilisation presented a serious threat for extended performance at $I_p \gtrsim 5$MA. In order to control this instability, two courses have been adopted: increased speed of amplifier response and active shape control. In addition, as a further safety measure, the vacuum vessel mounting has been recently strengthened, and hydraulic dampers fitted to control torsional movements. Future ohmic heating experiments will extend measurements to plasmas which fill the vessel cross-section (at higher elongations) and at larger plasma currents (up to the full planned value $I_p = 4.8$MA).

IV PLASMA DIAGNOSTICS

Table II lists the diagnostics presently in operation, and Fig. 2 indicates the layout and disposition of the various equipment on the machine. Table III provides a further list of diagnostics which are under construction and the dates by which these will come into operation. Further details of the diagnostics are available in Refs. [3] and [4].

V PLASMA PERFORMANCE

Basic Performance

Most of the early experiments were carried out in hydrogen and more recent data has been taken in deuterium. Plasma break-down is normally achieved with <20V/turn, with no preionization. At 3.5×10^{-5} mbar gas prefill pressure, a hot ($\sim$ 1keV) peaked temperature profile is produced after about 300ms. At lower filling pressures, the temperature profile is hollow, and often mini-disruptions are observed. Subsequently, additional impurities enter the discharge, probably due to magnetic reconnection. At higher filling pressures, a cold peaked temperature profile is produced; disruptions are observed, probably as the density limit is exceeded. Figure 3 shows the time dependence of plasma current, loop voltage and average density for a typical shot.

A survey of results under various conditions is given in Table IV, which represents data taken within a wide range of circuit and plasma parameters: $I_p < 3.7$MA; $1.3\text{T} < B_T < 3.4\text{T}$; $2.3 < q < 10$; $1.2 < b/a < 1.6$. The plasma shape is determined from the magnetic data. Near-circular plasmas ($b/a \sim 1.2$) and strongly elliptic plasmas ($b/a = 1.6$) have been established in both hydrogen and deuterium with long flat tops (up to 10s) in both current and density. Loop voltages on axis have been as low as 0.5V consistent with high central temperatures. The line average densities (obtained from the 2mm interferometer) vary in the range $1\text{-}3.5 \times 10^{19}$ m^{-3}.

Plasma Optimization

Much attention has been devoted to optimization of plasma in the ohmic heating phase, in which studies have been undertaken on the four phases: start-up, current rise, flat-top and termination. Considerable attention was applied to the elimination of stray fields during start-up. Two techniques were used

successfully on JET to enhance current penetration on JET during current rise: these were to increase the plasma cross-section and to ramp the toroidal field as the plasma current was increased, which allowed the current to be carried to the plasma centre even when formed at the edge, However, during the exploration of new operating regimes, current skins have been formed during the current rise and current rearrangements have lead to major disruptions. Special recovery procedures are necessary due to the increased impurity content of subsequent discharges causing difficulty in start-up. Recovery has been accomplished by using a low prefill pressure, to avoid cooling of the discharge by impurities and low plasma currents to minimize effects of further disruptions. During the current-rise and flat top, gas is bled into the chamber to increase the plasma density. However, there is a maximum density set by the disruption limit, proportional to the plasma current density. The driving voltage is removed at the end of the flat top and the plasma current is allowed to decay resistively (over a period of $\sim$ 10s). The plasma current normally decays smoothly, but for some high density flat-top pulses, the density can hold up in the decay, exceeding the high density limit and disruptions have occurred.

The overall JET results are shown on the Hugill-Murakami plot in Fig. 4, of normalized plasma current $1/q_{cyl}$ ($= \mu_o RI_p/2\pi B_T ab$) versus normalised density ($\bar{n}R/B_T$). At a fixed $\bar{n}R/B_T$, the maximum current is bounded by low q disruptive instabilities corresponding to a q_{cyl} of 2-3, while for a given value of q, there is another type of disruption at the density limit given by $\bar{n}R/B_T = A/q_{cyl}$ (where A is a constant depending on the purity of the plasma). This gives the relationship $\bar{n}(max) \propto \bar{j}$, where $\bar{j}$ is the average current density.

Impurity Studies

One of JET's main aims is to investigate the effects of impurities and the subsequent radiation losses from the plasmas, using visible and VUV spectroscopy, and bolometer and soft X-ray signals. O, C, wall metals (Ni, Cr and Fe) and Cl were identified as the main impurities in early plasmas. The graphite limiters are the main source of C and the walls appear to play a dominant role for O impurities. Metals are deposited on the limiter surfaces in the course of operations. Subsequently, limiter sputtering is the main source of metals in the plasma. Metal densities increased with I_p and decreased with plasma density, while light impurities were relatively insensitive to these parameters and depended more on the state of the vessel. This led to the tendency for Z_{eff} to fall with density, as shown in Fig. 5. During this period, bolometric measurements showed that 70-100% of the input power was radiated.

In order to reduce this radiation, a layer of lower Z material, carbon, was desposited on the vessel wall by glow discharge cleaning in a mixture of methane and hydrogen. This reduced the metals content immediately, by about a factor of 5, but this content recovered subsequently as the carbonization surface was removed or aged. In addition, Cl and O gradually decreased during the carbonization process, while the C fraction increased. The radiated power dropped as low as 40% and a considerable heat load on the limiters resulted. Due to the reduction of O and Cl, values of Z_{eff} reduced to $\sim$ 2.5, consisting of about 2% C, 1% O, 0.05% Cl and 0.015% metals. The density limit increased marginally, and by removing the remaining O it might increase further. Subsequently, further carbon tiles have been fitted to the inboard vacuum vessel wall.

Confinement Properties and Scaling Laws

Scans of density, current and toroidal field have been carried out during the various phases of operation to obtain information on scaling of energy and particle confinement times. These were carried out at constant plasma major and horizontal minor radius but with varying elongation factors (b/a) in the range 1.2 to 1.6.

The energy confinement time, τ_E, was determined from the relationship

$$\tau_E = \frac{3}{2} \int (n_e T_e + n_i T_i)\, dV/P_\Omega$$

where P_Ω is the total ohmic input power. The ion deficiency factor is $n_i/n_e = (Z_i + 1^\Omega - Z_{eff})/Z_i$, where Z_i is the charge of the principal impurity. In all calculations, the electron temperature profile was taken from the E.C.E. measurements, the density profile was that measured by the microwave reflectometer, the ion temperature was taken from the neutral particle analyser and the neutron yield monitors and spectrometers (in deuterium). τ_E was found to increase with density, as shown in Fig. 6, which shows data separated into four groups: hydrogen and deuterium; before and after carbonization. Improved values of τ_E were found in deuterium, after carbonization. Analysis has show that a good parameter fit is obtained between τ_E and nq_{cyl}. This is shown plotted in Fig. 6 as the dotted line. For comparison, data from PLT and TFTR are shown (including the aR^2 dependence, which has not been checked on JET.

Measurements of the radial variation of ohmic input power and radiated power are shown in Fig. 6 for both metal wall and carbonized wall situations. A detailed analysis of the local power balance shows that for the central region (to r/a = 0.75), radial transport is dominated by thermal conduction, and in the outer region, radiation dominates. Measurement accuracy does not permit a determination of whether the main loss mechanism in the centre is due to electrons or ions. If the ion thermal conduction, χ_i is neoclassical, then the electron thermal conductivity, χ_e, scales inversely with density, n.

From the previous density limit scaling $\bar{n}R/B_T = Aq_{cyl}$, taken with the expression $\tau_E \propto \bar{n}\, q_{cyl}$, gives the maximum value for the Lawson product $(\hat{n}\hat{\tau}_E)$ as:

$$(\hat{n}\hat{\tau}_E)_{max} \propto B_T^2/q_{cyl}$$

In Fig. 7, the Lawson diagram shows $(\hat{n}_i\hat{\tau}_E)$ plotted against the central ion temperature $\hat{T}_i$. The crosses indicate recent JET data, as compared with predictions for the various phases of JET operation (Table V) [5]. From the relationship, it can be seen that the best performance should be obtained at the highest plasma currents, which is consistent with the results.

Preliminary RF Studies

Recently two different prototype antennae have been installed in JET, allowing tests at ion cyclotron resonance frequencies (ICRF). Plasma coupling has been measured in various antenna configurations and under different conditions (varying density and antenna-plasma distance). To date, the power to a single antenna has been gradually increased to 2MW (for 1s) or 1.5MW (for 3s); a further increase to $\sim$ 4MW with 2 antennae will be undertaken shortly. Selected experimental plasma conditions have included the He^3 minority in a D_2 plasma (B_T = 3.4T, I_p = 2.8MA) and H minority in D_2 (B_T = 2.5T, I_p = 2.3MA).

Heating has been observed, but it is premature to report in more detail on these results at this stage.

VI SUMMARY OF CONCLUSIONS

From these initial results, the main conclusions are summarized as follows:

a) This large machine behaves in a similar way to smaller Tokamaks, particularly in formation of the discharge and subsequent behaviour of the plasma. The expected advantage of size is seen in the record energy confinement time;

b) Long duration discharges have been obtained (up to 20s) without disruptions, even during the current decay;

c) Plasma elongations in the range 1.2 to 1.6 have been successfully achieved, controlled by the feedback system. Loss of feedback control of the vertical position has occurred at higher elongations, as predicted;

d) High central electron temperatures (T_e up to 5keV) and ion temperatures (T_i up to 3keV) have been achieved in Ohmically heated plasmas with power inputs less than 3MW, although Z_{eff} was in the range 3-10;

e) The energy confinement time (τ_E) is better than extrapolation of INTOR scaling for a given plasma density and values up to 0.8s in D have been obtained;

f) As expected impurity levels present a problem. Early experiments showed high levels of radiated power, which could be attributed to radiation from a mixture of metallic impurities (i.e. nickel, etc..) from the centre and also from low-Z impurities (i.e. carbon, oxygen, etc...) from the edge. Later experiments with low-Z (carbon) tiles on the inner walls and a carbonized vessel showed reduced levels of metals and oxygen, resulting in lower Z_{eff} values and decreased radiation losses;

g) Initial experiments on ICRF heating have shown that MW power levels may be coupled to the plasma. Further experiments will concentrate on increasing this level and investigating the location and nature of the power deposition and its effect on temperature and confinement.

VII FUTURE EXPERIMENTS

Impurity Control

The recent experiments with increased carbon tile protection plates on the in board walls of the vessel, combined with carbonization of the vessel, have shown decreased metal impurities and lower Z_{eff} values. This suggests improved plasma performance with only low-Z material facing the plasma, (including the limiters and most of the vessel walls). Only two materials appear practicable: carbon and beryllium. Coinciding with the introduction of further additional heating power on JET, two toroidal belt limiters (toroidal rings situated 1m above and below the equatorial mid-plane) made of plates of either carbon or beryllium inserted between cooled fins will be installed in the machine at the end of 1986.

Additional Heating

25MW of additional heating will be applied to JET in phases (see Table V): two Neutral Injectors will provide 10MW and RF Heating at the Ion Cyclotron

Resonance Frequency (ICRF) will provide a further 15MW in the plasma (30MW from the generators) from 10 antennae disposed around the torus.

The ICRF heating system, will be progressively upgraded both in power and in antenna design. There are several modes of heating, working either at the fundamental frequency of a minority species (e.g. ^{3}He in H and D in H), or at harmonics of the main ion species. The systems frequency range (25 to 55 MHz) covers the different modes for the plasma species considered (D, H, T, ^{4}He and ^{3}He). By 1987, the present experimental antennae will be replaced by six actively cooled models providing 9MW of heating in the plasma. Later, a total of ten antennae, providing 15MW, should be available.

The first neutral beam injector designed to deliver 5MW of 80keV neutral hydrogen particles into the plasma will be installed in 1985. The injector contains 8 ion sources, and ion beam pulses of 80keV and 60A have been produced according to specification. Beam heated plasmas should be produced in late 1985. Manufacture of all components for the second injector are well advanced and this should be installed in 1986. It is planned to change to deuterium later, and a prototype source has already produced a beam of 160keV deuterons to the required specification.

Preparation for Tritium Operation

During 1989-90, facilities for the study of α-particle heating in D-T plasmas should be available. Basic decisions concerning the on-site hydrogen isotope separation plant have already been made. The plant will be based on gas chromatography and will allow recirculation of tritium into the vessel. Remote handling facilities are also in preparation for progressive use as machine activation increases, first due to deuterium operation and later in D-T experiments.

VIII ACKNOWLEDGEMENTS

The technical situation and the plasma results summarised here have been achieved by the combined work of the JET team, the Associated laboratories and European industry.

IX REFERENCES

(1) The JET Project - Design Proposal - Report of the Commission of the European Communities, EUR 5516e (EUR-JET-R5) (1976);

(2) Duesing G, Proc IX Inter. Vacuum Congress, Madrid (1983) p. 518;

(3) Rebut P H et al, Proc 10th IAEA Int. Conf on Plasma Phys and Controlled Fusion, (London, UK) Vol I p.11 (1984);

(4) JET Progress Report 1983: EUR 9472 (EUR-JET-PR1) (1984);

(5) Gibson A, Proceedings of 1984 Int. Conf on Plasma Physics, (Lausanne, Switzerland) Vol I, p.13 (1984);

TABLE I - Principal Parameters of JET

Parameter	Value
Maximum plasma minor radius (horizontal), a	1.25m
Maximum plasma minor radus (vertical), b	2.10m
Plasma major radius, R_o	2.96m
Plasma aspect ratio, R_o/a	2.37
Plasma elongation ratio, e=b/a	1.68
Flat top pulse length	up to 20s
Toriodal magnetic field (plasma centre)	3.45T
Plasma current: circular plasma;	3.2MA
D shaped plasma;	4.8MA
Volt-seconds available	34 Vs
Toroidal field peak power	380 MW
Poloidal field peak power	300 MW
Additional heating power (in plasma)	25 MW
R F Power	15 MW
Neutral beam power	10 MW

TABLE II - DIAGNOSTICS OPERATIONAL

Diagnostic	Purpose
Bolometer Scan	Time and space resolved total radiated power
Magnetic Diagnostics	Plasma current, loop volts, plasma position, shape of flux surfaces
Single Point Thomson Scattering	T_e and n_e at one point several times
Multichannel Far Infrared Interferometer	$\int n_e(r)ds$ on 7 vertical and 3 horizontal chords
Single Channel 1 mm and 2 mm Interferometer	$\int n_e(r)ds$ on 1 vertical chord in low density plasmas ($< 10^{-19} m^{-3}$)
Microwave Reflectometer	n_e profiles and fluctuations
Hard X-ray Monitors	Runaway electrons and disruptions
Soft X-ray Diode Arrays	MHD instabilities and location of rational surfaces
Electron Cyclotron Emission Spatial Scan	$T_e(r,t)$ with scan time of a few ms
Electron Cyclotron Emission Fast System	$T_e(r,t)$ on μs time scale
Limiter Surface Temperature	(i) Temperature of wall and limiter surfaces (ii) Monitor of hot spots on limiter
2.4 MeV Time-of-Flight Neutron Spectrometer	Neutron spectra in D-D discharges, Ion temperatures and energy distributions.
Time Resolved Neutron Yield Monitor	Time resolved neutron flux
Neutral Particle Analyser Array	Profiles of ion temperature
H_α and Visible Light Monitors	Ionization rate, Z_{eff}, Impurity fluxes
VUV Spectroscopy Spatial Span	Time and space resolved impurity densities
VUV Broadband Spectroscopy	Impurity Survey
Visible Spectroscopy	Impurity Fluxes from wall and limiters
Plasma Boundary Probe	Simplified probe system for monitoring progress of discharge cleaning and preliminary plasma-wall interaction experiments

TABLE III - DIAGNOSTICS UNDER CONSTRUCTION

Diagnostic	Purpose	Date for operation in JET
X-ray Pulse Height Spectrometer	Plasma purity monitor and T_e on axis	Mid 1984 (Provisional system) Mid 1985 (Full system)
2.4 MeV Neutron Spectrometer	Neutron spectra in D-D discharges, Ion temperatures and energy distributions	Mid 1985
Neutron Activation	Absolute fluxes of neutrons	Mid 1985
Neutron Yield Profile Measuring System	Space and time resolved profile of neutron flux	Mid 1985
Active Phase Spectroscopy	Impurity behaviour in active conditions	Early 1986
Spatial Scan X-ray Crystal Spectroscopy	Space and time resolved impurity density profiles	Early 1986
Grazing Incidence Spectroscopy	Impurity survey	Early 1986
High Resolution X-ray Crystal Spectroscopy	Ion temperature by line broadening	Mid 1985
Surface Analysis Station	Plasma-wall and limiter interactions including release and hydrogen isotope recycling	Mid 1985
Surface Probe Fast Transfer System		Mid 1985
Pellet Injector Diagnostic	Particle Transport, fuelling	Late 1985
Lidar Thomson Scattering	T_e and n_e profiles	*In design: If approved, installation by Early 1987

TABLE IV

TYPICAL JET DISCHARGE PARAMETERS FOR HYDROGEN (H) AND DEUTERIUM (D)

Pulse No.	I_p(MA)	B_T(T)	b/a	Cross-Sectional Area (m^2)	$\frac{\int ndl}{\int dl}$(x $10^{19} m^{-3}$)	$\hat{T}_e$(keV)	$\bar{Z}_{eff}$ (Brems)	τ_E(s)
1353 (H)	2.3	2.5	1.18	4.3	1.62	1.78	3.8	0.16
1356 (H)	3.0	2.5	1.25	4.6	1.80	2.00	5.0	0.18
1650 (H)	2.3	2.5	1.22	4.5	1.41	2.80	7.2	0.22
1695 (H)	2.1	2.5	1.21	4.4	2.30	2.00	5.1	0.33
1894 (H)	2.1	2.5	1.20	4.4	2.11	1.94	3.2	0.28
1955 (H)	1.7	2.6	1.63	7.0	0.69	3.35	9.5	0.23
2014 (H)	2.7	2.1	1.56	6.4	2.19	1.64	4.2	0.28
2019 (H)	2.4	2.6	1.51	6.2	1.81	2.30	4.0	0.31
2029 (H)	3.1	2.6	1.56	6.4	1.93	2.50	5.6	0.20
2471 (H)	3.0	3.4	1.20	5.0	2.84	2.46	4.1	0.40
2523 (D)	3.2	3.4	1.20	5.0	3.01	2.86	4.0	0.50
2534 (D)	2.1	2.5	1.20	4.8	2.12	2.33	2.5	0.42
2891 (H)	2.8	3.4	1.41	5.8	2.76	2.90	3.4	0.55
3049 (D)	3.6	3.4	1.45	6.3	2.95	3.43	3.4	0.72
3889 (D)	2.0	3.4	1.69	7.7	1.34	4.42	3.4	0.85
3899 (D)	1.0	3.4	1.54	6.7	0.84	4.32	3.9	0.72
3909 (D)	3.5	3.4	1.54	6.6	3.65	3.33	2.4	0.85

TABLE V

Phases in the Operation of JET

Phase		Effective Heating Power (above Ohmic)	Description	Objective
I (Ohmic Heating Studies)	mid 83	0	Commissioning: initial operation ohmic only.	Establish target plasma for heating (Hydrogen/Deuterium)
IIA	early 85	6 MW	6 MW ICRH. 5 MW 80 keV(H) heating (∿ 9 MW)	Impurity control. Density limits.
IIB (additional Heating Phase)	mid 86	16 MW	Progressively increase 10 MW 80 keV(H) +	Compare with theory. (Hydrogen/Deuterium)
III (Full Power Optimization)	1988	19 MW	Increase heating to full level including 10 MW (17 MW total) 160 keV D for D-T plasma	Establish limits to to performance. Compare with theory. Decide if D-T is justified. Commission D-T systems.
		25 MW	+ 15 MW ICRH (30 MW total)	(Deuterium)
IV (Tritium Phase)	1989	25 MW	D-T operation with α-heating dominant at least near axis.	Study approach to ignition. Study plasmas with profile set by α-heating. Find β limit in this system. (Deuterium/Tritium)

+ Effective Heating Power is taken to be the power in the highest energy component of the Neutral Injection plus 50% of the ICRH power coupled to the antenna.

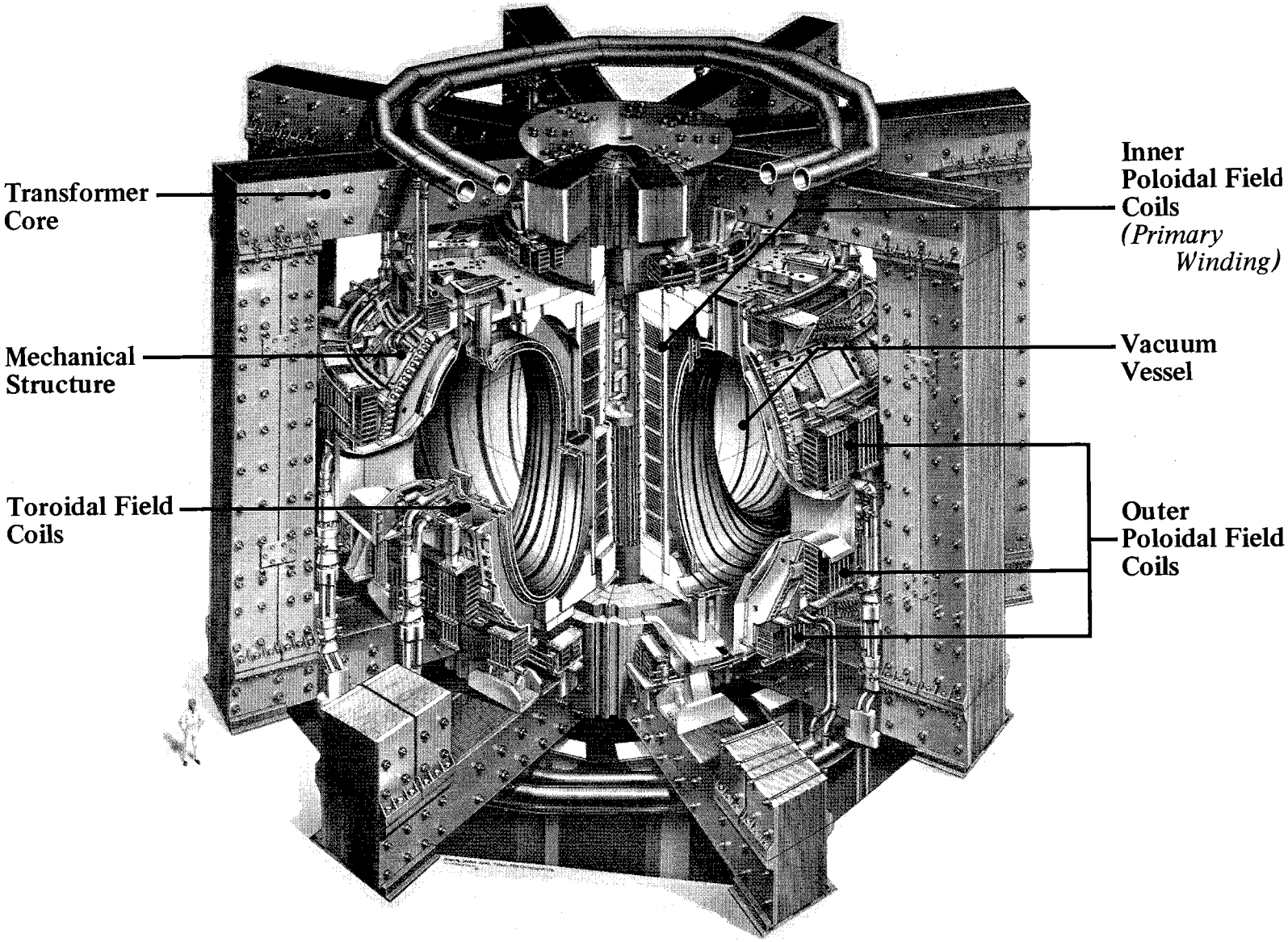

Fig. 1. Diagram of the JET tokamak.

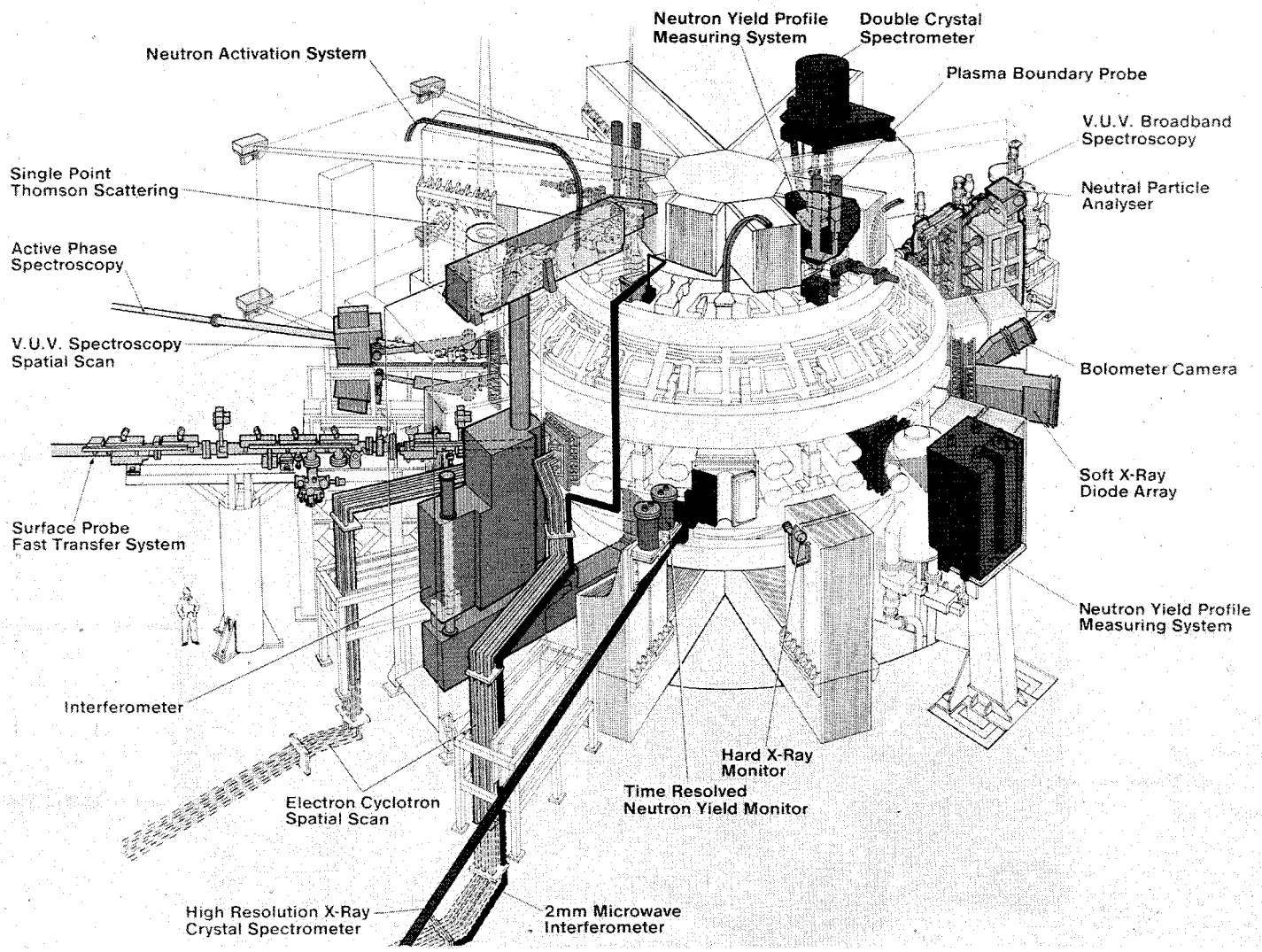

Fig. 2. Layout of diagnostics in the machines.

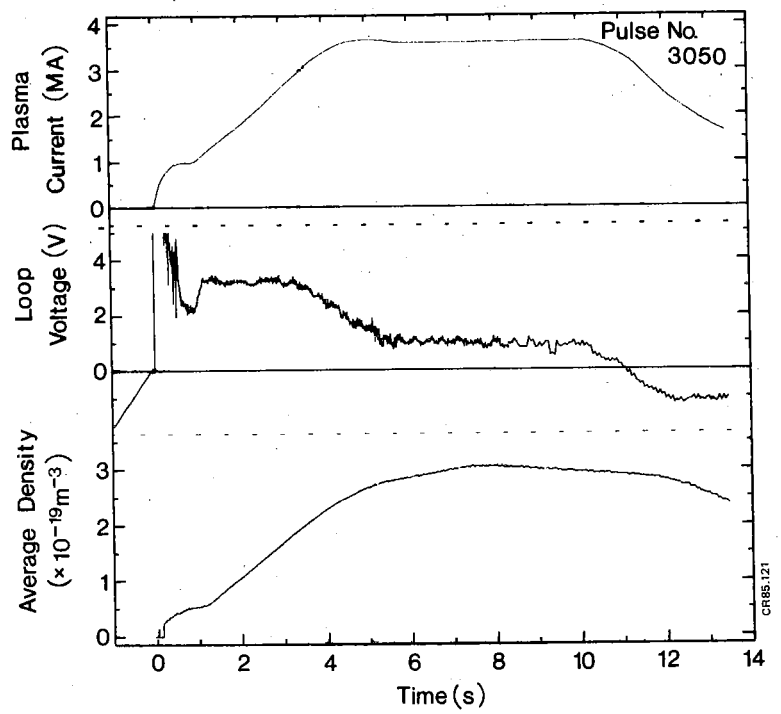

Fig. 3. Time dependance of plasma current I_p, loop voltage V_l and average electron density $\bar{n}_e$ for a typical JET pulse.

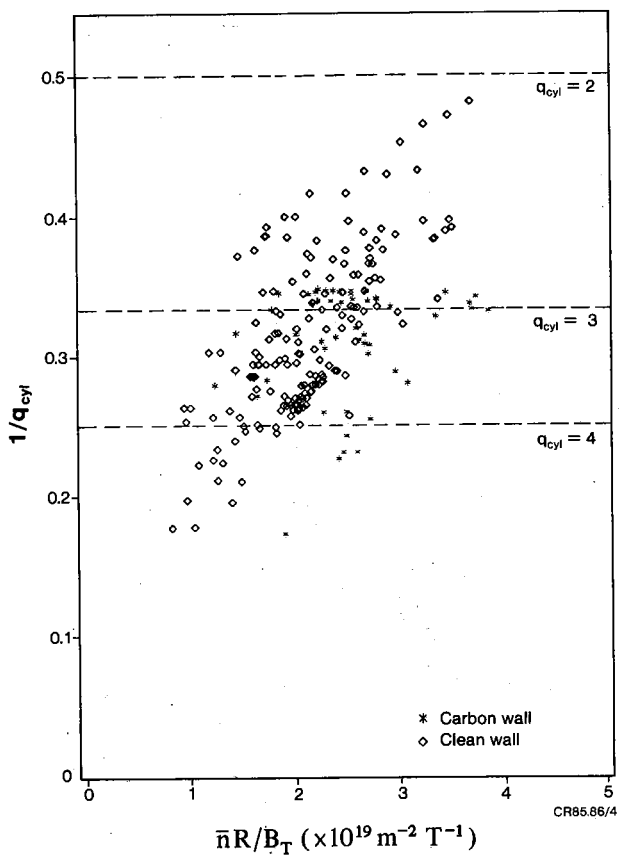

Fig. 4. Hugill-Murakami plot of $1/q_{cyl}$ versus $\bar{n}\,R/B_T$ for clean and carbonised walls.

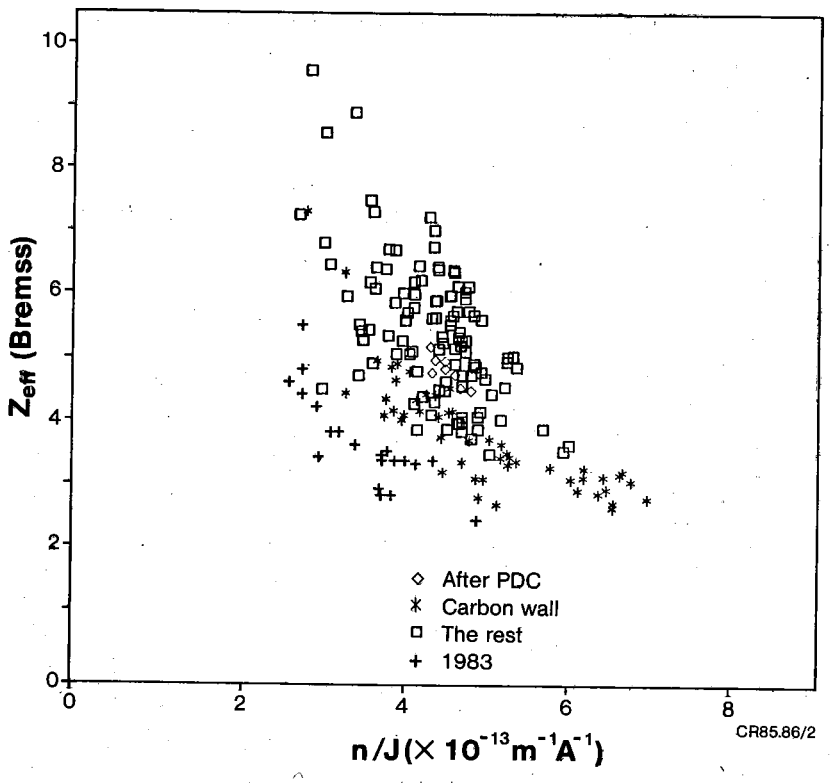

Fig. 5. Z_{eff} as a function of electron density n_e.

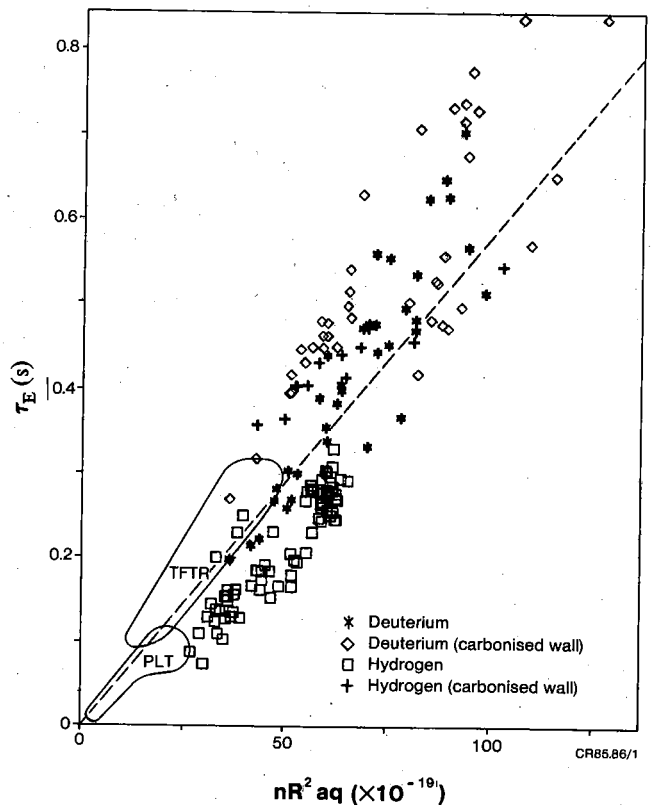

Fig. 6. Energy confinement time, τ_E, versus normalized density $\bar{n}\ R^2\ aq$, (Including data from PLT and TFTR).

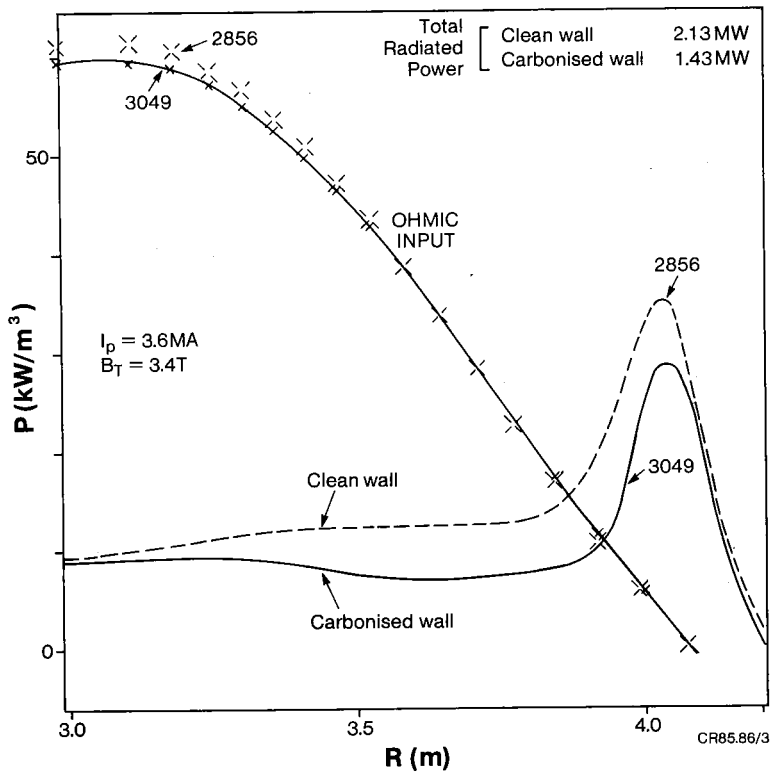

Fig. 7. Local power input and radiation as a function of radius, under conditions for a clean wall and for a carbonized wall.

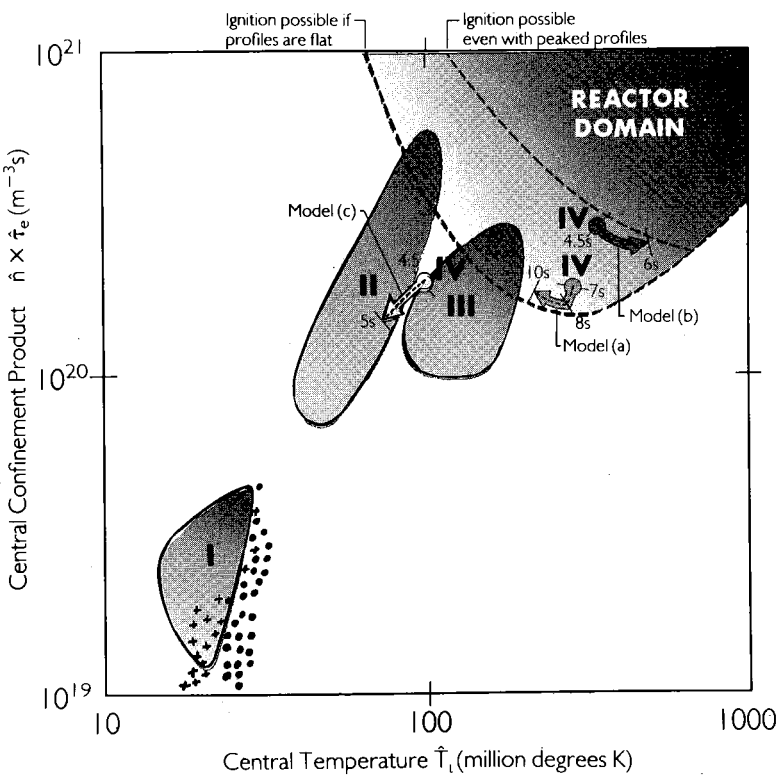

Fig. 8. Lawson diagram plot of $\langle \hat{n}_i \tau_E \rangle$ versus central ion temperature $\hat{T}_i$. The crosses show the recently achieved values in JET and the areas marked I, II, III, and IV show the regions of parameter space predicted for the various phases of JET operation (see Table V).

$+$ $I_p < 3$MA, $\bullet$ $I_p > 3$MA.